

Generalization of the theory of three-dimensional quantum Hall effect of Fermi arcs in Weyl semimetal

Mingqi Chang(苌名起), Yunfeng Ge(葛云凤), and Li Sheng(盛利)

Citation: Chin. Phys. B, 2022, 31 (**5**): 057304. DOI: 10.1088/1674-1056/ac5c32
Journal homepage: http://cpb.iphy.ac.cn; http://iopscience.iop.org/cpb

What follows is a list of articles you may be interested in

Quantum transport signatures of non-trivial topological edge states in a ring-shaped Su-Schrieffer-Heeger double-chain system

Cheng-Zhi Ye(叶成芝), Lan-Yun Zhang(张蓝云), and Hai-Bin Xue(薛海斌)
Chin. Phys. B, 2022, 31 (**2**): 027304. DOI: 10.1088/1674-1056/ac34ff

Topology of triple-point metals

Georg W. Winkler, Sobhit Singh, Alexey A. Soluyanov
Chin. Phys. B, 2019, 28 (**7**): 077303. DOI: 10.1088/1674-1056/28/7/077303

Scanning tunneling microscopic investigation on morphology of magnetic Weyl semimetal $YbMnBi_2$

Zhen Zhu(朱朕), Dong Yan(严冬), Xiao-Ang Nie(聂晓昂), Hao-Ke Xu(徐豪科), Xu Yang(杨旭), Dan-Dan Guan(管丹丹), Shiyong Wang(王世勇), Yao-Yi Li(李耀义), Canhua Liu(刘灿华), Jun-Wei Liu(刘军伟), Hui-Xia Luo(罗惠霞), Hao Zheng(郑浩), Jin-Feng Jia(贾金锋)
Chin. Phys. B, 2019, 28 (**7**): 077302. DOI: 10.1088/1674-1056/28/7/077302

Tunable Weyl fermions and Fermi arcs in magnetized topological crystalline insulators

Junwei Liu(刘军伟), Chen Fang(方辰), Liang Fu(傅亮)
Chin. Phys. B, 2019, 28 (**4**): 047301. DOI: 10.1088/1674-1056/28/4/047301

Topological transport in Dirac electronic systems: A concise review

Hua-Ding Song(宋化鼎), Dian Sheng(盛典), An-Qi Wang(王安琦), Jin-Guang Li(李金光), Da-Peng Yu(俞大鹏), Zhi-Min Liao(廖志敏)
Chin. Phys. B, 2017, 26 (**3**): 037301. DOI: 10.1088/1674-1056/26/3/037301

RAPID COMMUNICATION

Generalization of the theory of three-dimensional quantum Hall effect of Fermi arcs in Weyl semimetal

Mingqi Chang(苌名起)[1], Yunfeng Ge(葛云凤)[1], and Li Sheng(盛利)[1,2,†]

[1] *National Laboratory of Solid State Microstructures and Department of Physics, Nanjing University, Nanjing* 210093, *China*
[2] *Collaborative Innovation Center of Advanced Microstructures, Nanjing University, Nanjing* 210093, *China*

(Received 27 December 2021; revised manuscript received 16 February 2022; accepted manuscript online 10 March 2022)

The quantum Hall effect (QHE), which is usually observed in two-dimensional systems, was predicted theoretically and observed experimentally in three-dimensional (3D) topological semimetal. However, there are some inconsistencies between the theory and the experiments showing the theory is imperfect. Here, we generalize the theory of the 3D QHE of Fermi arcs in Weyl semimetal. Through calculating the sheet Hall conductivity of a Weyl semimetal slab, we show that the 3D QHE of Fermi arcs can occur in a large energy range and the thickness dependences of the QHE in different Fermi energies are distinct. When the Fermi energy is near the Weyl nodes, the Fermi arcs give rise to the QHE which is independent of the thickness of the slab. When the Fermi energy is not near the Weyl nodes, the two Fermi arcs form a complete Fermi loop with the assistance of bulk states giving rise to the QHE which is dependent on the sample thickness. We also demonstrate how the band anisotropic terms influence the QHE of Fermi arcs. Our theory complements the imperfections of the present theory of 3D QHE of Fermi arcs.

Keywords: Weyl semimetal, three-dimensional quantum Hall effect, Fermi arcs

PACS: 73.23.−b, 73.50.−h, 73.43.−f **DOI:** 10.1088/1674-1056/ac5c32

1. Introduction

Quantum Hall effect (QHE), which is discovered in two-dimensional (2D) electron gases, opens a new era of condensed matter physics.[1–5] To generalize the QHE to three-dimensional (3D) systems, tremendous effort has been made.[6–15] Recently, the 3D QHE has been theoretically predicted to occur in Weyl semimetals.[16–18] Weyl semimetals are new topological states of matter of which low-energy bulk excitations can be explicited by Weyl equations.[19–28] The energy spectrums of Weyl equations touch at discrete points, called Weyl nodes. The topologically protected surface states between the Weyl nodes form Fermi arcs, which are the landmark feature of Weyl semimetals.[19] In a Weyl semimetal, the Fermi arcs at two opposite surfaces can be connected by the Weyl nodes via a "wormhole" tunneling, forming a complete Fermi loop producing the QHE.[16] Following the prediction, the quantized Hall plateaus have been experimentally observed in the 3D topological semimetal Cd_3As_2.[29–35] In Ref. [16], the Fermi arcs can support the QHE only when the Fermi energy is at Weyl nodes and the band anisotropy terms exist, which is hardly achievable. Meanwhile, the thickness dependence of Fermi-arc 3D QHE is unclear. However, Ref. [30] showed that the quantum Hall resistance is sensitive to the sample thickness. These contradictions between theory and experiments suggest that the present theory of the 3D QHE of Fermi arcs is imperfect.

In this paper, we generalize the theory of the 3D QHE of Fermi arcs in Weyl semimetal. Through calculating the sheet Hall conductivity of a Weyl semimetal slab, we show that the 3D QHE of Fermi arcs can occur in a large energy range and the thickness dependences of the QHE in different Fermi energies are distinct. When the Fermi energy is near the Weyl nodes, the Fermi arcs from two surfaces form a complete Fermi loop needed by QHE. The Fermi arcs give rise to the QHE which is independent of the thickness of the slab. In this case, the anisotropic terms are necessary, or the QHE cannot occur. When the Fermi energy is not at the Weyl nodes and is not out of the energy range of Fermi arc states, the Fermi arcs at two surfaces form a complete Fermi loop with the assistance of bulk states. The Fermi arcs and bulk states give rise to the QHE together which is dependent on the sample thickness. The anisotropic terms are not necessary in this case. The Fermi arc surface states are essential in both two cases. When the Fermi energy is out of the energy range of Fermi arcs, only the bulk states contribute to the Hall conductivity destroying the quantized plateaus of QHE. Our theory complements the imperfections of the present theory of 3D QHE of Fermi arcs.

The rest of the paper is organized as follows. In Section 2, we introduce the model Hamiltonian. In Section 3, we plot the energy spectrum for bulk states and Fermi arc states, and make a brief analysis according to the energy spectrum. In Section 4, the sheet Hall conductivities in different Fermi en-

[†]Corresponding author. E-mail: shengli@nju.edu.cn

© 2022 Chinese Physical Society and IOP Publishing Ltd

ergies are calculated numerically when a y direction magnetic field $\boldsymbol{B} = (0, B, 0)$ is applied. The final section contains a brief summary.

2. Model

We consider a 3D model of Weyl semimetal with two Weyl nodes,[16,36–40]

$$H = D_1 k_y^2 + D_2(k_x^2 + k_z^2) + A(k_x\sigma_x + k_y\sigma_y) + M(k_w^2 - \boldsymbol{k}^2)\sigma_z, \tag{1}$$

where $(\sigma_x, \sigma_y, \sigma_z)$ are the Pauli matrices, $\boldsymbol{k} = (k_x, k_y, k_z)$ is the wave vector, and D_1, D_2, A, M and k_w are the model parameters. D_1 and D_2 are anisotropic terms. This model contains all the topological properties of Weyl semimetals.[40] The energy dispersion of this model is

$$\begin{aligned} E_{\pm}^{\boldsymbol{k}} &= D_1 k_y^2 + D_2(k_x^2 + k_z^2) \\ &\pm \sqrt{A^2(k_x^2 + k_y^2) + M^2(k_w^2 - \boldsymbol{k}^2)^2}, \end{aligned} \tag{2}$$

with $\pm$ for the conductance and valence bands. The model has two Weyl nodes at $\boldsymbol{k}_{\pm} = (0, 0, \pm k_w)$ with the same energy $E_w = D_2 k_w^2$.

The effective Hamiltonian of Fermi arc states in a Weyl semimetal slab has been calculated in Ref. [16]. The effective Hamiltonian of the Fermi arc on the $y = L/2$ surface is

$$H_{\text{arc}} = vk_x + D_1 k_w^2 + (D_2 - D_1)(k_x^2 + k_z^2), \tag{3}$$

with $v = A\sqrt{M^2 - D_1^2}/M$. The Fermi arc at the $y = L/2$ surface is confined in a region defined by the constraint

$$ak_x + k_x^2 + k_z^2 < k_w^2, \tag{4}$$

with $a = AD_1/M\sqrt{M^2 - D_1^2}$. Similarly, the effective model of the Fermi arc state at the opposite surface of the Weyl semimetal slab is

$$H'_{\text{arc}} = -vk_x + D_1 k_w^2 + (D_2 - D_1)(k_x^2 + k_z^2). \tag{5}$$

The Fermi arc at this surface is confined in a region defined by the constraint

$$-ak_x + k_x^2 + k_z^2 < k_w^2. \tag{6}$$

3. Energy spectrum

In Figs. 1(a) and 1(b), we plot the energy spectra for bulk states and Fermi arc surface states of the Weyl semimetal as functions of k_x and k_z with different anisotropic D terms. The Fermi arc states are plotted as blue and pink curves while the bulk states are plotted as red curves. In Fig. 1(a), when the anisotropic terms are $D_1 = D_2 = 0$, the Fermi arc states disperse linearly with k_x while the Fermi arc is not in Fig. 1(b), when the anisotropic terms are $D_1 = 2$ eV·nm^2 and $D_2 = 3$ eV·nm^2.

In Figs. 1(c) and 1(e), we plot the Fermi arc states and bulk states on the plane of k_x and k_z for $D_1 = D_2 = 0$ eV·nm^2. When the Fermi energy is precisely at the Weyl nodes, the Fermi arc states of the two surfaces on the plane of k_x and k_z form a straight line as shown in Fig. 1(c). However, when the Fermi energy is not at Weyl nodes, the Fermi arcs at opposite surfaces can form a complete Fermi loop with the assistance of bulk states in Fig. 1(e).

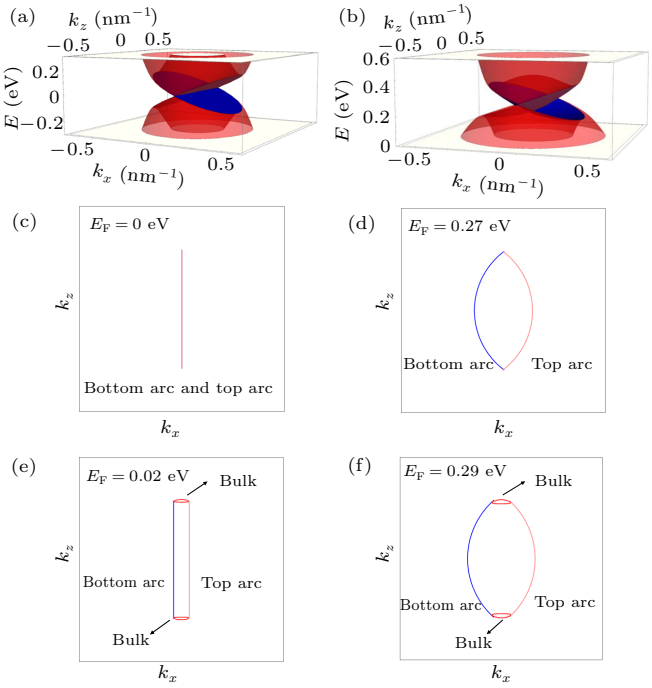


Fig. 1. (a) and (b) Energy spectra for bulk states and Fermi arc states with (a) $D_1 = D_2 = 0$ eV·nm^2, (b) $D_1 = 2$ eV·nm^2, $D_2 = 3$ eV·nm^2. (c)–(f) Fermi arc states and bulk states on the plane of k_x and k_z for different Fermi energy. In (c) $E_F = 0$ eV and (e) $E_F = 0.02$ eV, the anisotropic terms are $D_1 = D_2 = 0$ eV·nm^2. In (d) $E_F = 0.27$ eV and (f) $E_F = 0.29$ eV, the anisotropic terms are $D_1 = 2$ eV·nm^2, $D_2 = 3$ eV·nm^2. The blue curves and pink curves are the Fermi arc states plotted using Eqs. (3) and (5) while the bulk states are plotted as red curves using Eq. (2).

In Figs. 1(d) and 1(f), the situation is different when the anisotropic terms are $D_1 = 2$ eV·nm^2 and $D_2 = 3$ eV·nm^2. In Fig. 1(d), the Fermi arcs at two surfaces can form a complete Fermi loop themselves when the Fermi energy is precisely at Weyl nodes. When the Fermi energy is not at Weyl nodes, the Fermi arcs at two surfaces form a complete Fermi loop with the assistance of bulk states as shown in Fig. 1(f).

We can make a brief analysis according to Fig. 1. First, when the Fermi energy is at Weyl nodes, the Fermi arcs at opposite surfaces can form a complete Fermi loop needed by QHE only when the anisotropic terms exist. Second, when the Fermi energy is not at Weyl nodes, the Fermi arcs at two surfaces form a complete Fermi loop with the assistance of bulk states no matter the anisotropic terms exist or not. Therefore, the Fermi arcs in Weyl semimetal can give rise to the QHE in a large energy range. On the one hand, when the Fermi energy is at Weyl nodes and the anisotropic terms exist, the Fermi arcs at two opposite surfaces form a complete Fermi loop giving rise

to the QHE. Because the Fermi arcs are independent of the sample size, the QHE is independent of the thickness of the sample in this case. On the other hand, when the Fermi energy is not at Weyl nodes, the Fermi loop needed by QHE is formed by the cooperation of Fermi arc states and bulk states. In this situation, the QHE is dependent on the thickness of the sample because the bulk states are size dependent. In the following, we calculate the Hall conductivity of a Weyl semimetal slab to verify our analysis.

4. Hall conductivity

We numerically calculate the Hall conductivity of a Weyl semimetal slab in a magnetic field using the Kubo formula[14–16]

$$\sigma_{\rm H} = \frac{e^2\hbar}{{\rm i}V_{\rm eff}} \sum_{\delta,\delta'\neq\delta} \frac{\langle\Psi_\delta|v_x|\Psi_{\delta'}\rangle\langle\Psi_{\delta'}|v_z|\Psi_\delta\rangle[f(E_{\delta'})-f(E_\delta)]}{(E_\delta - E_{\delta'})(E_\delta - E_{\delta'} + {\rm i}\Gamma)}, \tag{7}$$

where $|\Psi_\delta\rangle$ is the eigenstate of energy E_δ for H in a y-direction magnetic field with open boundaries at $y = \pm L/2$, $V_{\rm eff}$ is the volume of the slab, v_x and v_z are the velocity operators, and $f(x)$ is the Fermi distribution.

The sheet Hall conductivity for the Weyl semimetal slab is defined by $\sigma_{\rm H}^{\rm s} = \sigma_{\rm H} L$. We numerically calculate the sheet Hall conductivity at zero temperature using the same method as in Refs. [16,41].

In Figs. 2(a) and 2(b), we show the sheet Hall conductivity as a function of Fermi energy $E_{\rm F}$ for different anisotropic terms and sample sizes. The sheet Hall conductivity is quantized in units of e^2/h no matter the anisotropic terms exist or not. However, the plateaus of sheet Hall conductivity are obviously different in Figs. 2(a) and 2(b). When the Fermi energy is near Weyl nodes, $\sigma_{\rm s}^{\rm H}$ is zero for $D_1 = D_2 = 0$ eV·nm^2 in Fig. 2(a) while $\sigma_{\rm s}^{\rm H}$ is nonzero for $D_1 = 2$ eV·nm^2, $D_2 = 3$ eV·nm^2 in Fig. 2(b). It means that the anisotropic terms are necessary for the QHE in Weyl semimetal when the Fermi energy is near the Weyl nodes. Moreover, when the Fermi energy is near Weyl nodes, $\sigma_{\rm s}^{\rm H}$ is independent of the thickness of the slab as shown in Fig. 2. When the Fermi energy is not near the Weyl nodes, the plateaus of sheet Hall conductivity depend on the sample size. The $\sigma_{\rm s}^{\rm H}$ is symmetric about the energy of Weyl nodes in Fig. 2(a) while is not in Fig. 2(b) because of the anisotropic terms.

In Fig. 3(a), we plot the sheet Hall conductivity in units of e^2/h as a function of $1/B$ when the Fermi energy is at Weyl nodes for different anisotropic terms. When $D_1 = D_2 = 0$ eV·nm^2, the top and bottom Fermi arcs coincide forming a straight line between two Weyl nodes as shown in Fig. 3(b), which cannot give rise to the QHE. Therefore, the $\sigma_{\rm H}^{\rm s}$ is zero as the red line in Fig. 3(a). However, the Fermi arcs at the two surface connected by Weyl nodes can form a complete Fermi loop needed by QHE when $D_1 = 2$ eV·nm^2, $D_2 = 3$ eV·nm^2 as shown in Fig. 3(b). The $\sigma_{\rm H}^{\rm s}$ is quantized in units of e^2/h as the green line shown in Fig. 3(a), which is the case in Ref. [16]. In this situation, the anisotropic terms are necessary for the QHE in Weyl semimetal.

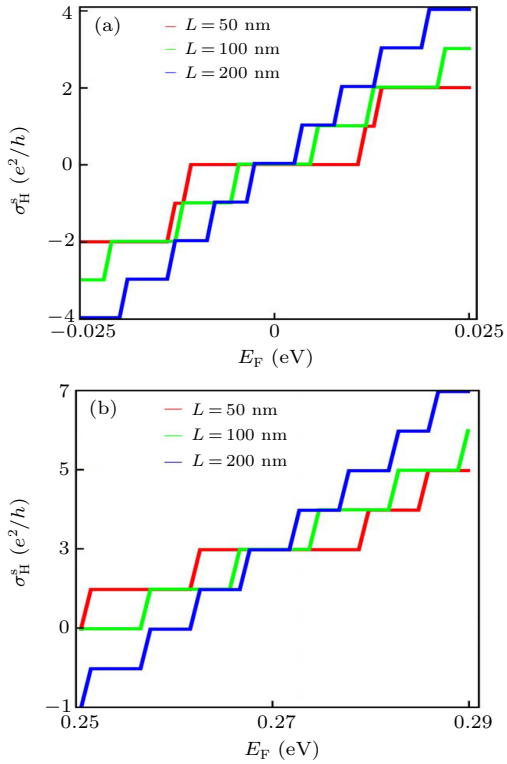


Fig. 2. In a Weyl semimetal slab, the sheet Hall conductivity in units of e^2/h as a function of Fermi energy with different thicknesses for $B = 5$ T. The anisotropic terms are (a) $D_1 = D_2 = 0$ eV·nm^2, (b) $D_1 = 2$ eV·nm^2, $D_2 = 3$ eV·nm^2. The parameters are $M = 5$ eV·nm^2, $A = 0.5$ eV·nm, and $k_{\rm w} = 0.3$ nm^{-1}.

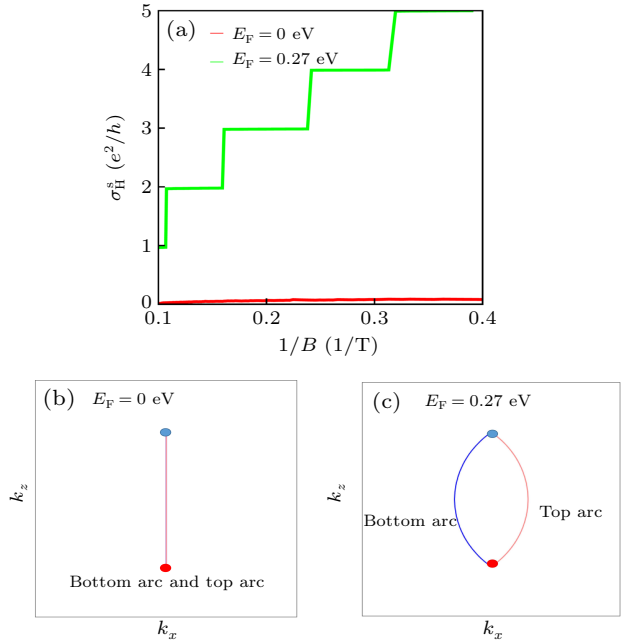


Fig. 3. When the Fermi energy is at Weyl nodes. (a) The sheet Hall conductivity $\sigma_{\rm s}^{\rm H}$ as a function of $1/B$ for $D_1 = D_2 = 0$ eV·nm^2 (red line), $D_1 = 2$ eV·nm^2, $D_2 = 3$ eV·nm^2 (green line). The thickness of the slab is $L = 100$ nm. Fermi arc states and bulk states on the plane of k_x and k_z for (b) $D_1 = D_2 = 0$ eV·nm^2, (c) $D_1 = 2$ eV·nm^2, $D_2 = 3$ eV·nm^2. The red point and blue point are Weyl nodes. The blue curves and pink curves are the Fermi arc states plotted using Eqs. (3) and (5). The other parameters can be found in Fig. 2.

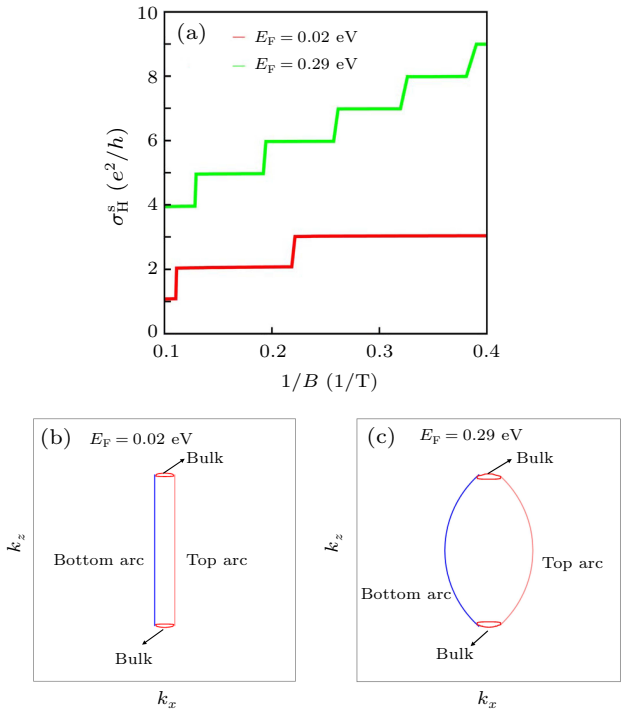


Fig. 4. (a) The sheet Hall conductivity σ_s^H as a function of $1/B$ for $D_1 = D_2 = 0$ eV·nm^2 (red line), $D_1 = 2$ eV·nm^2, $D_2 = 3$ eV·nm^2 (green line) and $L = 100$ nm. Fermi arc states and bulk states on the plane of k_x and k_z for (b) $D_1 = D_2 = 0$ eV·nm^2 at $E_F = 0.02$ eV, (c) $D_1 = 2$ eV·nm^2, $D_2 = 3$ eV·nm^2 at $E_F = 0.29$ eV. The other parameters can be found in Fig. 2.

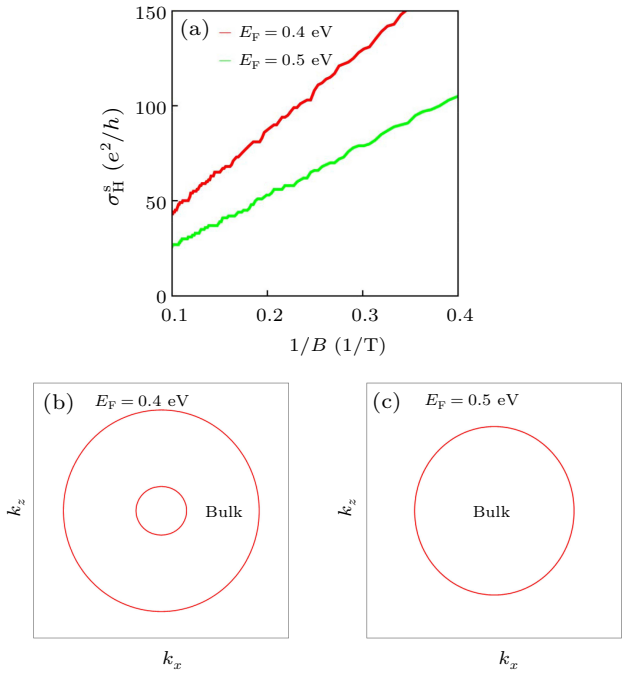


Fig. 5. (a) The sheet Hall conductivity σ_s^H as a function of $1/B$ for $D_1 = D_2 = 0$ eV·nm^2 (red line), $D_1 = 2$ eV·nm^2, $D_2 = 3$ eV·nm^2 (green line) and $L = 100$ nm. Fermi arc states and bulk states on the plane of k_x and k_z for (b) $D_1 = D_2 = 0$ eV·nm^2 at $E_F = 0.4$ eV, (c) $D_1 = 2$ eV·nm^2, $D_2 = 3$ at $E_F = 0.5$ eV. The other parameters can be found in Fig. 2.

We plot the sheet Hall conductivity in units of e^2/h as a function of $1/B$ when the Fermi energy is not at Weyl nodes in Fig. 4(a). In this case, the σ_H^s shows plateaus no matter the anisotropic terms exist or not. This can be seen from the Fermi arc states and bulk states on the plane of k_x and k_z. In Figs. 4(b) and 4(c), the Fermi arcs form a complete Fermi loop needed by QHE with the assistant of bulk states no matter the anisotropic terms exist or not. The QHE is generated under the combined action of bulk states and Fermi arc states. The Fermi loop in Fig. 4(c) is bigger than that in Fig. 4(b). This is why the green line is above the red line in Fig. 4(a).

In Fig. 5(a), when the Fermi energy is out of the energy range of the Fermi arc states, we plot the sheet Hall conductivity in units of e^2/h as a function of $1/B$ for different anisotropic terms. When the Fermi energy is out of the energy range of the Fermi arc states, the bulk states themselves form a complete Fermi loop as shown in Figs. 5(b) and 5(c). In this situation, only the bulk states contribute to the Hall conductivity. As like a normal metal, the sheet Hall conductivity follows the usual $1/B$ dependence in Fig. 5(a). Meanwhile, the Fermi loop in Fig. 5(b) is bigger than that in Fig. 5(c) causing the value of σ_H^s of red line above the green line in Fig. 5(a).

The above results of Hall conductivity are consistent with our analysis in Section 3.

5. Summary

In summary, we generalize the theory of the 3D QHE of Fermi arcs in Weyl semimetal. Through calculating the sheet Hall conductivity of a Weyl semimetal slab, we show that the 3D QHE of Fermi arcs can occur in a large energy range and the thickness dependences of the QHE in different Fermi energies are distinct. The position of Fermi energy plays an important role. When the Fermi energy is near the Weyl nodes, the Fermi arcs at two surfaces form a complete Fermi loop when the anisotropic terms exist giving rise to the QHE. The anisotropic terms are necessary for the QHE in this situation. In this situation, the QHE is independent of the sample size because the Fermi arc states are independent of the sample thickness. When the Fermi energy is not near the Weyl nodes and is not out of the energy range of Fermi arc states, the Fermi arcs form a complete Fermi loop with assistance of bulk states no matter the anisotropic terms exist or not. The QHE is generated under the combined action of bulk states and Fermi arc surface states. Because the bulk states depend on the thickness of the slab, the QHE is dependent on the sample size. Finally, when the Fermi energy is out of the energy range of Fermi arc states, only the bulk states contribute to the Hall conductivity. The plateaus of σ_H^s collapse and the σ_H^s follows the usual $1/B$ dependence as like a normal metal. In experiment, it is difficult to distinguish if it is the Fermi arcs producing the QHE in Weyl semimetal. Using our theory, this can be estimated through the different thickness dependence in different Fermi energies.

Acknowledgment

This work was supported by the National Natural Science Foundation of China (Grant No. 11974168) (L.S.).

References

[1] Klitzing K V, Dorda G and Pepper M 1980 *Phys. Rev. Lett.* **45** 494
[2] Novoselov K S, Geim A K, Morozov S V, Jiang D, Katsnelson M I, Grigorieva I V, Dubonos S V and Firsov A A 2005 *Nature* **438** 197
[3] Zhang Y, Tan Y W, Stormer H L and Kim P 2005 *Nature* **438** 201
[4] Yoshimi R, Yasuda K, Tsukazaki A, Takahashi K S, Nagaosa N, Kawasaki M and Tokura Y 2015 *Nat. Commun.* **6** 8530
[5] Thouless D J, Kohmoto M, Nightingale M P and denNijs M 1982 *Phys. Rev. Lett.* **49** 405
[6] Halperin B I 1987 *Jpn. J. Appl. Phys.* **26** 1913
[7] Kohmoto M, Halperin B I and Wu Y S 1992 *Phys. Rev. B* **45** 13488
[8] Koshino M , Aoki H, Kuroki K, Kagoshima S and Osada T 2001 *Phys. Rev. Lett.* **86** 1062
[9] Bernevig B A, Hughes T L, Raghu S and Arovas D P 2007 *Phys. Rev. Lett.* **99** 146804
[10] Störmer H, Eisenstein J, Gossard A, Wiegmann W and Baldwin K 1986 *Phys. Rev. Lett.* **56** 85
[11] Wang P, Ren Y, Tang F, Wang P, Hou T, Zeng H, Zhang L and Qiao Z 2020 *Phys. Rev. B* **101** 161201(R)
[12] Qin F, Li S, Du Z, Wang C, Zhang W, Yu D, Lu H Z and Xie X C 2020 *Phys. Rev. Lett.* **125** 206601
[13] Tang F, Ren Y, Wang P, Zhong R, Schneeloch J, Yang S A, Yang K, Lee P A, Gu G, Qiao Z, *et al.* 2019 *Nature* **569** 537
[14] Chen Rui, Wang C M, Liu Tianyu, Lu H Z and Xie X C 2021 *Phys. Rev. Research* **3** 033227
[15] Ma R, Sheng D and Sheng L 2021 *Phys. Rev. B* **104** 075425
[16] Wang C M , Sun H P, Lu H Z and Xie X C 2017 *Phys. Rev. Lett.* **119** 136806
[17] Lu H Z 2019 *National Science Review* **6** 208
[18] Chen Rui , Liu Tianyu, Wang C M, Lu H Z and Xie X C 2021 *Phys. Rev. Lett.* **127** 066801
[19] Wan X, Turner A M, Vishwanath A and Savrasov S Y 2011 *Phys. Rev. B* **83** 205101
[20] Burkov A A and Balents L 2011 *Phys. Rev. Lett.* **107** 127205
[21] Yang K Y, Lu Y M and Ran Y 2011 *Phys. Rev. B* **84** 075129
[22] Xu G, Weng H, Wang Z, Dai X and Fang Z 2011 *Phys. Rev. Lett.* **107** 186806
[23] Delplace P, Li J and Carpentier D 2012 *Europhys. Lett.* **97** 67004
[24] Jiang J H 2012 *Phys. Rev. A* **85** 033640
[25] Singh B, Sharma A, Lin H, Hasan M, Prasad R and Bansil A 2012 *Phys. Rev. B* **86** 115208
[26] Liu J and Vanderbilt D 2014 *Phys. Rev. B* **90** 155316
[27] Bulmash D, Liu C X and Qi X L 2014 *Phys. Rev. B* **89** 081106(R)
[28] Armitage N, Mele E and Vishwanath A 2018 *Rev. Mod. Phys.* **90** 015001
[29] Zhang C, Narayan A, Lu S, Zhang J, Zhang H, Ni Z, Yuan X, Liu Y, Park J H, Zhang E, *et al.* 2017 *Nat. Commun.* **8** 1272
[30] Zhang C, Zhang Y, Yuan X, Lu S, Zhang J, Narayan A, Liu Y, Zhang H, Ni Z, Liu R, *et al.* 2019 *Nature* **565** 331
[31] Nishihaya S, Uchida M, Nakazawa Y, Kriener M, Kozuka Y, Taguchi Y and Kawasaki M 2018 *Sci. Adv.* **4** eaar5668
[32] Uchida M, Nakazawa Y, Nishihaya S, Akiba K, Kriener M, Kozuka Y, Miyake A, Taguchi Y, Tokunaga M, Nagaosa N, *et al.* 2017 *Nat. Commun.* **8** 2274
[33] Schumann T, Galletti L, Kealhofer D A, Kim H, Goyal M and Stemmer S 2018 *Phys. Rev. Lett.* **120** 016801
[34] Kealhofer D A, Galletti L, Schumann T, Suslov A and Stemmer S 2020 *Phys. Rev. X* **10** 011050
[35] Lin B C, Wang S, Wiedmann S, Lu J M, Zheng W Z, Yu D and Liao Z M 2019 *Phys. Rev. Lett.* **122** 036602
[36] Zhang S B, Lu H Z and Shen S Q 2016 *New J. Phys.* **18** 053039
[37] Shen S Q 2012 *Topological Insulators* (Berlin Heidelberg: Springer-Verlag)
[38] Sun H P and Lu H Z 2019 *Frontiers of Physics* **14** 33405
[39] Okugawa R and Murakami S 2014 *Phys. Rev. B* **89** 235315
[40] Lu H Z, Zhang S B and Shen S Q 2015 *Phys. Rev. B* **92** 045203
[41] Chang M and Sheng L 2021 *Phys. Rev. B* **103** 245409